Transistor Switches using Active Piezoelectric Gate Barriers

Raj K. Jana, Arvind Ajoy, Gregory Snider, and Debdeep Jena

arXiv:1505.00378v1 [cond-mat.mes-hall] 2 May 2015

***Abstract*—This work explores the consequences of introducing a piezoelectric gate barrier in a normal field-effect transistor. Because of the positive feedback of strain and piezoelectric charge, internal charge amplification occurs in such an electromechanical capacitor resulting in a negative capacitance. The first consequence of this amplification is a boost in the on-current of the transistor. As a second consequence, employing the Lagrangian method, we find that by using the negative capacitance of a highly compliant piezoelectric barrier, one can potentially reduce the subthreshold slope of a transistor below the room temperature Boltzmann limit of 60 mV/decade. However, this may come at the cost of hysteretic behavior in the transfer characteristics.**

***Index Terms*—Electrostriction, Electromechanical capacitor, Piezoelectric barrier, Negative capacitance, PiezoFET, Subthreshold slope**

I. Introduction

SCALING of the size of field-effect transistors (FETs) has improved their performance and integration densities in integrated circuits for over two decades. Most conventional transistors make use of a passive insulating barrier layer between the gate metal and the semiconductor channel to modulate the density of conduction channel electrons or holes. Because the intrinsic properties of a passive gate barrier do not change with the applied voltage, they impose certain fundamental limitations on the resulting device performance.

One such limitation is the subthreshold slope, i.e. the gate voltage required to change the drain current by an order of magnitude [1], [2], given by $SS = m \times 60$ mV/decade at room temperature [3], [4]. Here, $m = 1 + C_{sc}/C_{ins}$ is the 'body factor', C_{sc} is the semiconductor channel capacitance, and C_{ins} is the gate insulator capacitance. In a traditional FET switch with a passive gate dielectric such as SiO_2, $C_{ins} > 0$ and thus $m > 1$, which leads to $SS > 60$ mV/decade [4]. This result, combined with circuit requirements for the on current I_{on} and the on/off ratio I_{on}/I_{off} establish a minimum supply voltage V_{dd}, which does not scale in direct proportion with feature size [1], [2], [5]. Scaling of V_{dd} has hit a roadblock, giving rise to heat generation associated with the large power dissipation density in ICs [1], [2], [6], [5], since the dissipated power is proportional to the square of the voltage, $P_{diss} \propto V_{dd}^2$ [2], [7]. Many ideas based on alternate transport mechanisms in the semiconductor channel, such as interband tunneling, or impact ionization are being explored to lower V_{dd}.

An interesting alternative is to replace the passive gate barrier with an active one. A first proposal of an active ferroelectric insulator [3] predicts *internal voltage gain*: the voltage across the gate insulator layer is larger than the applied external gate voltage. The origin of internal voltage gain is the collective alignment of the microscopic electric dipoles in the ferroelectric layer in response to the external electric field produced by the gate voltage. The alignment of dipoles generates a voltage of its own, thus amplifying the voltage that makes it to the semiconductor channel. Under appropriate bias conditions [3], the insulator capacitance provided by the ferroelectric is mathematically negative ($C_{ins} < 0$), causing $m = 1 + C_{sc}/C_{ins} < 1$ and $SS < 60$ mV/decade. Such an active-gate FET then will require a lower gate voltage to create the same charge as a conventional FET with passive gate dielectrics [3], thereby facilitating device scaling.

In this paper, we explore the device consequences of using a *piezoelectric* insulator as the active gate barrier in a transistor instead of the ferroelectric barrier. Piezoelectric gate barriers are at the heart of commercially available III-nitride heterostructure transistors [8], [9]. We first consider an active compliant piezoelectric layer as the insulator in a parallel plate capacitor. We find that this simple electromechanical capacitor system exhibits a remarkably rich range of behavior. We show that negative capacitance emerges as a natural response to applied voltage. In this regime of negative capacitance, we show that we obtain a higher charge than in a corresponding capacitor with a passive dielectric. Non-trivial capacitance-voltage behavior in such capacitors have also been reported experimentally [10], [11]. Next, we port the parallel-plate electromechanical capacitor to the gate capacitor of a FET. We show how this piezoelectric gate stack enables a higher on-current than in a transistor with a passive dielectric due to internal charge amplification. Finally, building upon our earlier proposals [12], [13], [14], we discuss the possibility of using the negative capacitance regime of a highly compliant piezoelectric barrier to obtain sub-60 mV/decade switching in a transistor.

II. Electromechanical capacitor

We begin by discussing the piezoelectric parallel-plate capacitor. Consider the parallel plate capacitor of area A shown in Fig. 1 (a). The equilibrium thickness t_0 of the piezoelectric insulator layer sandwiched between the metal plates changes to $t = t_0 - \delta$ when a voltage V is applied on the plates, as shown in Fig. 1 (b). The strain is defined as $s = \delta/t_0$. The equal and opposite sheet charges σ_m that develop on the metal plates set up an attractive force between them, which strains the insulator. This effect, called electrostriction, is the electric-field

R. K. Jana, A. Ajoy, G. Snider, and D. Jena are with the Electrical Engineering Department, University of Notre Dame, Notre Dame, IN, 46556 USA e-mail: rjana1@nd.edu; aajoy@nd.edu; snider.7@nd.edu; djena@nd.edu.

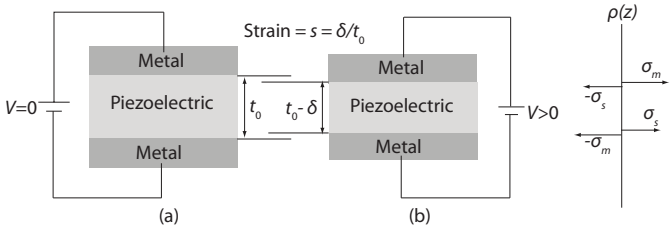

Fig. 1. (a) Schematic cross section of a parallel-plate electromechanical capacitor with piezoelectric barrier layer of thickness t_0 at $V = 0$ V, b) The layer thickness shrinks to $t_0 - \delta$ when voltage V is applied. Sheet charge distribution $\rho(z)$ with $\pm\sigma_m$ on the metal plates and surface charges $\pm\sigma_s$ on the piezoelectric.

induced reduction of the thickness of a material; it occurs in *all* insulators, whether or not the layer is piezoelectric. However if the insulator is piezoelectric, the strain *amplifies* the surface charge of the insulator. This mechanism sets up a positive feedback between the thickness and the electric field, and is responsible for the appearance of negative capacitance. To find the capacitance in the presence of such electromechanical coupling, one must first find the net metal charge σ_m as a function of the external (battery) voltage, and then take its derivative. This requires us to identify the surface charges σ_s that develop at the surface of the insulator. The resulting electric field profile is constant, equal to $E = V/t$, and the voltage drops linearly across the insulator.

Maxwell's boundary conditions across the metal-insulator interface requires the normal components of the displacement vector to obey $D_d - D_m = \sigma_m$. D_d is the displacement field in the dielectric related to the surface charges σ_s by $D_d = \epsilon_0 E + \sigma_s$, where $\sigma_s = (\epsilon_d - \epsilon_0)E + e_{33}s + \sigma_{sp}$ or $D_d = \epsilon_d E + e_{33}s + \sigma_{sp}$. Here $\epsilon_d = \epsilon_0(1 + \chi_d)$ is the net dielectric constant of the piezoelectric layer, and χ_d is its electric susceptibility. The electric field is $E = V/t$, where $t = t_0(1 - s)$ is the thickness of the *strained* insulator layer. We explicitly allow for both piezoelectric and spontaneous polarization for an active dielectric material. The strain-induced piezoelectric contribution to the charge (to linear order) is $e_{33}s$, where e_{33} is the piezoelectric coefficient in units of C/m^2 and $s = \delta/t_0$ is the strain along the field. The charge due to spontaneous polarization is σ_{sp}, also in units of C/m^2. Inside the metal, $D_m = 0$. Therefore, we obtain the relation

$$\sigma_m = \epsilon_d \frac{V}{t_0(1-s)} + e_{33}s + \sigma_{sp}. \tag{1}$$

This relation illustrates how the strain s explicitly enters the *electrostatic* relation between the metal charge and the voltage across the capacitor. If one neglects the spontaneous polarization ($\sigma_{sp} \to 0$), piezoelectric effect ($e_{33} \to 0$) and strain ($s \to 0$), we get $\sigma_m = C_0 V$, (with $C_0 = \epsilon_d/t_0$), the standard textbook formula of a parallel plate capacitor. However, we note that one can turn off the spontaneous and piezoelectric polarization by choice of material, and yet the factor $(1 - s)$ in the denominator will persist: this is the electrostriction term.

The mechanical pressure P experienced by the insulator is the electrical force F per unit area A. It is thus related to the metal charge [15], [16] via $P = F/A = \sigma_m^2/\epsilon_d$. To linear order, the pressure depends on the strain via the stiffness coefficient $P = C_{33}s$, where C_{33} is in units of N/m^2, or Pascals. Thus, we obtain the strain as a function of the metal charge: $s = \sigma_m^2/\epsilon_d C_{33}$. Substituting in Eq. 1 and rearranging, we have the desired relation between the metal charge in response to an applied voltage:

$$C_0 V = \sigma_m - \sigma_{sp} + \frac{(\sigma_{sp} - e_{33})}{\epsilon_d C_{33}}\sigma_m^2 - \frac{1}{\epsilon_d C_{33}}\sigma_m^3 + \frac{e_{33}}{(\epsilon_d C_{33})^2}\sigma_m^4. \tag{2}$$

The right hand side is a fourth order polynomial in σ_m, and captures the electromechanical coupling physics. Let us explore its consequences. The sheet charge on the metal $n_m = \sigma_m/q$ from Eq. 2 is plotted as a function of the applied voltage V in Fig. 2 for different sets of material parameters. For example, $e_{33} = 3.1$ C/m^2, $\epsilon_d = 15\epsilon_0$ correspond to the piezoelectric material $Sc_xAl_{1-x}N$ [17], [18]. The value of C_{33} is allowed to vary arbitrarily in order to investigate the range of behavior of the piezoelectric capacitor. We also assume $\sigma_{sp} = 0$. A non-zero value of σ_{sp} merely causes a horizontal shift of the $\sigma_m - V$ curve (see Supporting document). The physics of the piezoelectric capacitor with $\sigma_{sp} = 0$ becomes apparent by factoring Eq. 2 into

$$V = \frac{q}{C_0}(n_m)\left(1 - \frac{n_m}{n_\eta}\right)\left(1 + \frac{n_m}{n_\eta}\right)\left(1 - \frac{n_m}{n_\pi}\right), \tag{3}$$

where $qn_m = \sigma_m$, $qn_\pi = \epsilon_d C_{33}/e_{33}$, and $qn_\eta = \sqrt{\epsilon_d C_{33}}$. Setting $V = 0$ in Eq. 3, we obtain four *real* roots $n_{m0} = 0$, $+n_\eta$, $-n_\eta$ and $+n_\pi$. For a rigid ($C_{33} \to \infty$), non-piezoelectric ($e_{33} = 0$) insulator, $n_\eta, n_\pi \to \infty$, whereupon we recover $\sigma_m = qn_m = C_0 V$, and the metal charge is a linear function of voltage as shown in the green line in Fig. 2(a).

On the other hand, for a compliant non-piezoelectric insulator, $C_{33} > 0$, and Eq. 3 reduces to a cubic equation with roots $0, \pm n_\eta$ at $V = 0$. This is in fact a prototypical description of a nano-electromechanical switch [19]. The two additional roots $\pm n_\eta$ make the dependence of σ_m on V *nonlinear* with two additional zero crossings. Multiple zero crossings of the $qn_m - V$ curve mathematically guarantees that there must be regions of negative slope $d(qn_m)/dV < 0$. This is shown in red in the flipped S-shaped curve of Fig. 2(a), where $C_{33} = 1$ GPa is assumed. In these regions, the electromechanical capacitor has a negative capacitance.

However, the negative capacitance corresponds to very high values of charge density($> 10^{14}$ cm^{-2}) and strain s (> 0.3), as shown in Fig. 3(a). Though rapid progress is being made in the solid-state electrostatic gating of ever increasing carrier densities in semiconductors [20], methods to reduce the charge and strain are desirable. Now consider the piezoelectric insulator where $C_{33} > 0$ and $e_{33} > 0$. Notice that n_η is independent of e_{33}. The root n_π depends on e_{33} and its location determines the shape of the $qn_m - V$ curve. If $e_{33} > \sqrt{\epsilon_d C_{33}}$, then $0 < n_\pi < n_\eta$ and negative capacitance appears in the two charge segments $[n_1 = -n_\eta, n_2]$ and $[n_3, n_4]$ shown in red in Fig. 2. It is important to realize that piezoelectricity lowers both the charge density ($\sim 10^{13}$ cm^{-2}) [inset of Fig. 2(a)] and strain < 0.01 [Fig. 3(b)] at which negative capacitance

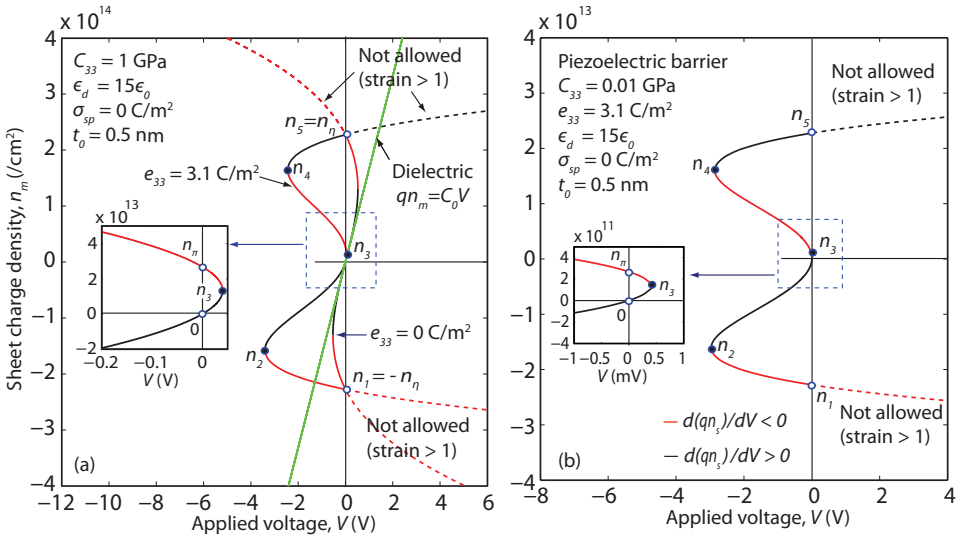

Fig. 2. a) Charge-voltage ($qn_m - V$) characteristic of the electromechanical capacitor. Various charge states such as the positive capacitance segments $[n_2, n_3]$, $[n_4, n_5]$ where the slopes $C_{PE} = d(qn_m)/dV > 0$ are positive, and negative capacitance segments $[n_1, n_2], [n_3, n_4]$ where $C_{PE} = d(qn_m)/dV < 0$ are shown, b) The characteristics of a piezoelectric capacitor with a lower stiffness and more compliant barrier with $C_{33} = 0.01$ GPa makes negative capacitance accessible at a lower charge $\sim 10^{11}$ cm^{-2}, as shown in the inset.

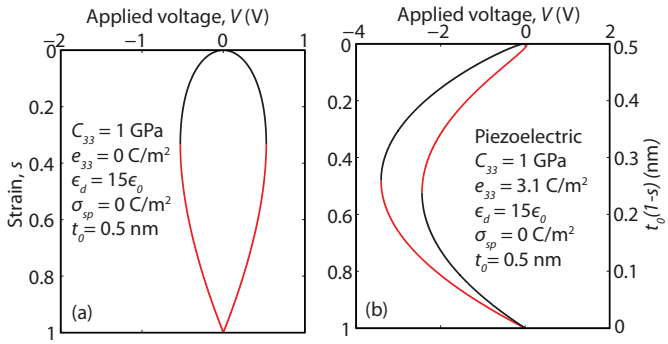

Fig. 3. Strain as a function of voltage in a) a non-piezoelectric insulator layer with $C_{33} = 1$ GPa, $e_{33} = 0$ C/m^2, $t_0 = 0.5$ nm, and b) in a piezoelectric insulator layer with $C_{33} = 1$ GPa, $e_{33} = 3.1$ C/m^2. Strain $s < 1$ is physically accessible in solid state, where the remaining layer thickness, $t_0(1-s) > 0$. Red (black) represents strain corresponding to the negative (positive) capacitance charge states.

appears, compared to electrostriction alone. For vanishingly small voltages around zero, the piezoelectric capacitor behaves exactly like a parallel plate capacitor - a straight line. But the additional benefit of the above coupling is the increased charge density compared to a passive dielectric due to the piezoelectric amplification - this effect will boost the on-state current in a transistor. From Eq. 3, the piezoelectric amplification is $n_m - \frac{C_0 V}{q} \approx \frac{n_m^2}{n_\pi} + \ldots$ to leading order. Finally, if we use a highly compliant piezoelectric, for example with $C_{33} = 0.01$ GPa, negative capacitance can be accessed at very low charge density $\sim 10^{11}$ cm^{-2}, as indicated in Fig. 2(b). These highly compliant piezoelectrics can potentially enable the design of transistors with steep sub-threshold behavior, but require new materials as will be described later. We also remark here that Pauli's exclusion principle of solid matter and quantum compressibility restricts $s < 1$. Therefore for piezoelectric insulators, the metal charge will be restricted to $-n_\eta < n_m < +n_\eta$. It may be possible to go beyond these restrictions ($s > 1$, shown as dashed lines in Fig. 2) in gaseous plasmas where charged ion plate 'electrodes' can pass through each other. But we do not pursue that line of analysis here, by restricting the discussion to solid metals and dielectrics.

III. Transistor with a Piezoelectric Barrier

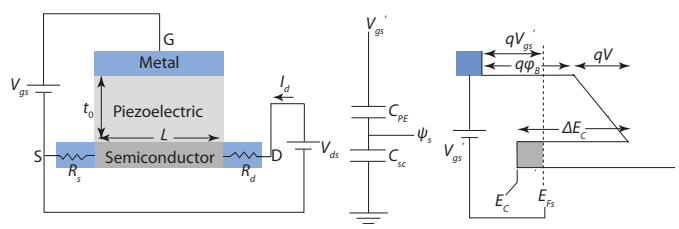

Fig. 4. Schematic cross section of a transistor ("piezoFET") with a piezoelectric gate barrier, semiconductor channel such as Si, GaN or 2D material, MoS_2, and source and drain ohmic contacts. The gate capacitance circuit is a series combination of the piezoelectric capacitance C_{PE} and the semiconductor capacitance C_{sc}. Here intrinsic gate voltage $V'_{gs} = V_{gs} - I_d Rs$, and intrinsic drain voltage $V'_{ds} = V_{ds} - I_d(R_s + R_d)$, where R_s and R_d are the source and drain contact resistances. The energy band diagram is shown for the metal-piezoelectric-semiconductor stack of the transistor. $\psi_s = V'_{gs} - V = (E_{Fs} - E_C)/q$ is the surface potential.

We now explore how the presence of the piezoelectric capacitor in the gate of a transistor with a semiconductor channel changes the traditional characteristics. The semiconductor channel could be formed of a gapped 2-dimensional crystal such as MoS_2, or a 3-D crystal semiconductor such as Si or GaN. The semiconductor is characterized by the valley degeneracy g_v of the conduction (or valence) band. We assume the energy dispersion of each valley to be the same, characterized by an effective mass $m^\star$ and spin degeneracy $g_s = 2$. Carrier transport in the semiconductor channel is assumed to be 2-dimensional - which holds both for monolayer 2D crystals and in field-effect transistors made of 3D semiconductors,

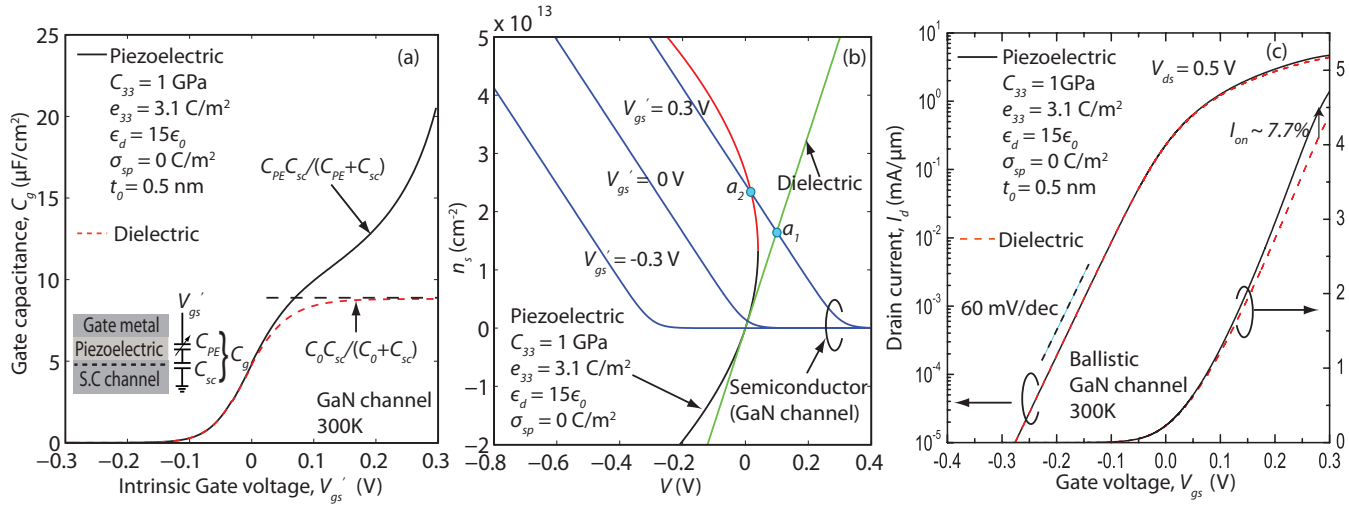

Fig. 5. a) Gate capacitance C_g versus V'_{gs} for transistors with piezoelectric (solid line) and dielectric (dashed line) insulators, b) Graphical load line analysis to obtain sheet carrier density n_s for different V'_{gs}. Blue curves show the semiconductor charge for different V'_{gs}, green shows the metal charge in the case of a passive dielectric, whereas red(black) shows the metal charge in the negative(positive) capacitance regimes of the piezoelectric capacitor. Intersections a_1 and a_2 of the above characteristics define the operating points of the system, c) Transfer curve depicts the drain current I_d versus V_{gs} at drain voltage $V_{ds} = 0.5$ V for GaN transistors with piezoelectric (solid line) and dielectric barriers (dashed line).

where transport occurs in a quasi-2D electron/holes gas. The occupation of multiple 2D subbands can then be treated as individual 2D channels - we consider a single subband model.

The semiconductor channel of length L and width W is assumed to be connected to very low-resistance ohmic contacts at the source and drain, as shown in Fig. 4. The energy-band diagram in Fig. 4 shows the potential barrier controlled by the voltage on the gate metal. Electrical charge neutrality requires $\sigma_m = qn_s$, where n_s is the mobile carrier sheet density at the 'top-of-the-barrier' in the energy band diagram along the length of the channel. The energy band diagram from the metal to the semiconductor requires $q\phi_B + qV - \Delta E_c + (E_{Fs} - E_c) = qV'_{gs}$. By suitable choice of materials, we assume that $q\phi_B = \Delta E_c$; if this is not the case, the difference can be absorbed in a shift of threshold voltage. When no drain voltage is applied, carriers in the semiconductor are in thermal equilibrium with the source and drain reservoirs, which for a parabolic 2D bandstructure means $qn_s = C_{sc}V_{th}\ln(1+\exp[(E_{Fs}-E_c)/kT])$, or $E_{Fs} - E_c = kT\ln(\exp[qn_s/C_{sc}V_{th}] - 1)$, where $C_{sc} = q^2 g_s g_v m^\star/2\pi\hbar^2$ is the density of states semiconductor capacitance, and the thermal voltage $V_{th} = kT/q$. From the energy band diagram in Fig. 4, the relation between the applied gate voltage V'_{gs} and the voltage drop V across the piezoelectric insulator is $qV'_{gs} = qV + (E_{Fs} - E_C)$. Here, $(E_{Fs} - E_c)/q = (V'_{gs} - V) = \psi_s$ is the surface potential. Using the carrier density expression and Eq. 2, the gate-induced charge qn_s in the semiconductor channel is self-consistently calculated. Finally, using this new dependence of charge on the voltages and the piezoelectric coefficients, the current-voltage characteristics of the piezoFET are obtained from the ballistic transport model [21] incorporating the quantum contact resistances of 0.026 k$\Omega.\mu$m [22] at the source and drain ends.

Fig. 5 shows the gate capacitance $C_g = d(qn_s)/dV'_{gs}$, and device characteristics $(I - V)$ of a ballistic piezoFET with a GaN channel ($m^\star = 0.2\ m_0$, $g_v = 1$ [23]). Fig. 5(a) shows that a higher gate C_g is obtained in the piezoFET (solid line), as compared to a FET with a passive gate (dashed line). The higher C_g is due to the negative capacitance resulting from piezoelectric charge amplification: $C_{PE}C_{sc}/(C_{PE}+C_{sc}) > C_0C_{sc}/(C_0+C_{sc})$ when $C_{PE} < 0$. Fig. 5(b) depicts the solution of the piezoelectric and semiconductor charge equations graphically, following the load-line approach (see [24]). The blue lines depict charge in the semiconductor channel, and the green, black, and red lines depict the charge drawn into the metal from the battery. They must be equal to maintain global charge neutrality, meaning the locus of intersections are the operating points of the device. The green line is the charge on the metal for a traditional passive gate dielectric, and the red/black lines for a piezoelectric gate. When the transistor is on ($V'_{gs} \sim +0.3$ V), an increase in the charge at point a_2 in Fig. 5(b) is seen for the piezoelectric compared to point a_1 for a passive dielectric. This increased charge boosts the on-current as depicted in Fig. 5(c), consequently improving the I_{on}/I_{off} ratio. This sort of piezoelectric amplification is an interesting method to boost the on-current in *any* transistor. Since much of the high-performance characteristics such as gain and cutoff frequencies depend on I_{on}, corresponding boosts can be expected in these parameters. This may be specially useful for boosting the current in FETs made of relatively low mobility channel materials. Note however in Fig. 5(c) that this device still has a SS of 60 mV/decade. This is because the negative capacitance regime is only accessible for charge densities $\geq 1.5 \times 10^{13}$ cm^{-2}: at this high level of charge, the transistor is in its on-state, rather than in the sub-threshold regime.

Because the charge-voltage characteristic of the piezoelectric capacitor is highly non-linear, it can have multiple intersections with the semiconductor load line. Ref. [25] develops a systematic procedure to understand such non-linear systems

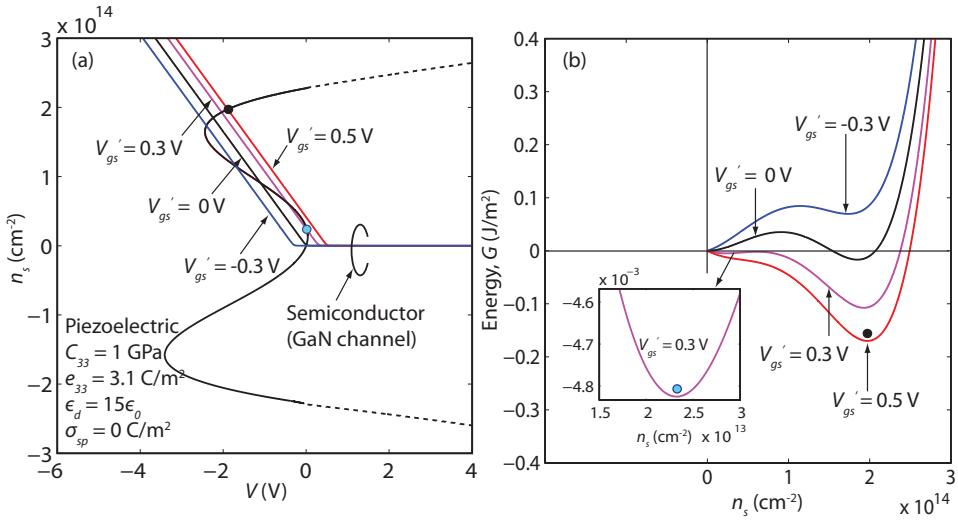

Fig. 6. a) Load line analysis showing multiple intersections of the piezoelectric and semiconductor characteristics for different V'_{gs}, b) Free-energy landscape of the piezoelectric-semiconductor stack at various V'_{gs}. Blue and black dots show stable operating points.

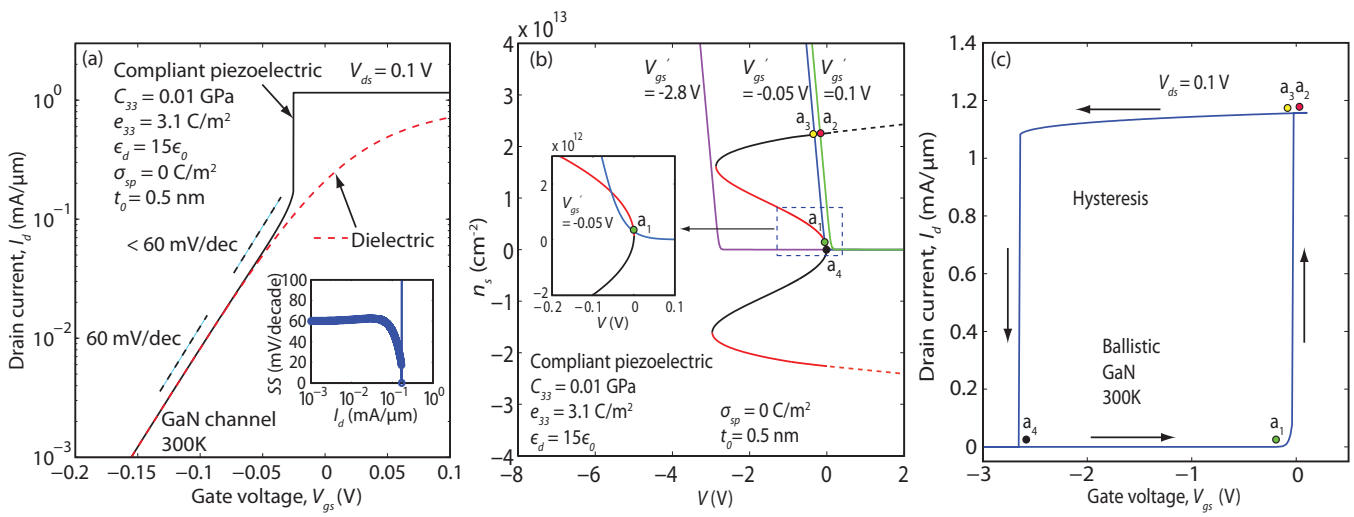

Fig. 7. a) I_d versus V_{gs} curves at $V_{ds} = 0.1$ V for a GaN channel piezoFET with a compliant piezoelectric with $C_{33} = 0.01$ GPa. A boost in the on-current and sub-60 mV/dec SS (inset) are obtained as compared to a passive gate dielectric. b) Load line characteristics to explain the hysteresis with gate bias voltages V'_{gs}, c) The calculated hysteresis in the transfer curve I_d versus V_{gs} for forward and reverse sweeps is shown for a GaN channel piezoFET.

based on the Euler-Lagrange equations of motion (see supporting document for details). For this analysis, we define a free-energy G in units of J/m^2 for the piezoelectric-semiconductor stack: $G(\sigma_m, V'_{gs}) = \int V d\sigma_m + \int \psi_s d\sigma_m - \sigma_m V'_{gs}$, where V is the voltage drop across the gate insulator and ψ_s is the surface potential. Minima in this free-energy landscape correspond to stable charge solutions of the non-linear system. If there are multiple minima, the actual solution $\sigma_m = qn_s$ depends on the previous state, or the *history* of the system.

For example, Fig. 6(a) shows the load lines and the corresponding evolution of the free-energy landscape for different V'_{gs} are shown in Fig 6(b). The shape of the energy landscape changes with the applied voltage. There are two energy minima in the range $-0.35 < V'_{gs} < 0.35$ V, and a single minimum otherwise. Let us assume that there is no charge to begin with on the capacitor, and ramp the gate from a negative to a positive voltage. Until around $V'_{gs} = +\,0.35$ V, the system remains in the minimum corresponding to the lower charge state ($\sim 2.3 \times 10^{13}$/cm^2) shown as a blue dot in Fig. 6(a) and the inset of Fig. 6(b). But when $V'_{gs} > 0.35$ V it is driven into the higher charge state shown as a black dot. Thus, provided $V'_{gs} < 0.35$ V, the transistor displays no hysteresis in its $I-V$ characteristics.

It is pertinent here to note an important difference in the nature of negative capacitance of the piezoelectric and ferroelectric insulators. The ferroelectric capacitor possesses negative capacitance at zero charge, whereas the capacitance of the piezoelectric capacitor is positive at zero charge. This property of the ferroelectric capacitor is exploited in achieving $SS < 60$ mV/decade, since the semiconductor load line can intersect the negative capacitance regime of the ferroelectric characteristic at the very low charge densities corresponding to

subthreshold operation of the transistor. Can a similar negative capacitance be obtained in the SS regime ($V'_{gs} < 0$ V) using piezoelectric gates? We explore this by tuning the piezoelectric material properties.

We find that if a lower stiffness, highly compliant piezoelectric barrier with $C_{33} \sim 0.01$ GPa is used, it can enable the reduction of the subthreshold slope below 60 mV/decade and also boost the on-current. This is shown in Fig. 7(a). Here negative capacitance is accessed in the subthreshold region, shown by the operating point a_1 in the load line characteristics at V'_{gs} = -0.05 V shown in Fig. 7(b). The on-state operation of this transistor corresponds to the higher charge state determined by the operating point a_2 in the load line characteristics at $V'_{gs} = 0.1$ V. However, this also results in hysteresis in the transistor characteristics with V'_{gs} sweep, as shown in the $I_d - V_{gs}$ characteristics in Fig. 7(c) which is calculated using the Lagrangian method. Hysteresis is undesirable in purely switching applications, but desirable for memory. Further, the strain in the higher charge states a_2, a_3 is very close to 100%, which is not feasible in realistic materials. If suitable new piezoelectric materials with ultra-low C_{33} and high e_{33} could be developed (see Supporting Information for various piezoelectrics with different C_{33} and e_{33}), sub-60 mV/decade switching can be achieved with hysteresis with suitable choice of semiconductors. Investigation of other transistor designs incorporating the piezoelectric barrier, such as the quantum metal transistor [26] to eliminate the hysteresis and reduce strain could be the focus of future work.

IV. Conclusion

We also emphasize that we have assumed linear piezoelectric parameters in this work to keep the model simple and yet capture the new physics. The non-linear material response needs to be explored in future. To conclude, the behavior of transistor switches using active piezoelectric gate barriers was explored. Because of electrostriction and piezoelectricity, negative capacitance is predicted to appear in a piezoelectric capacitor. Using this negative capacitance and a ballistic transport model, we predict that compliant piezoelectric barriers can boost the gate capacitance and increase the on-currents of transistors. Also, steep switching with sub-60 mV/decade subthreshold slope is predicted when the negative capacitance of the piezoelectric barrier is accessed in the off-state operation of the transistor, and this steep behavior is predicted to be assisted by hysteresis based on the Lagrangian method of stability of the transistor system.

Acknowledgment

This work was supported by the Center for Low Energy Systems Technology (LEAST), one of six centers of STARnet, the Semiconductor Research Corporation (SRC) program sponsored by MARCO and DARPA.

References

[1] L. Chang, D. Frank, R. K. Montoye, S. J. Koester, B. L. Ji, P. W. Coteus, R. H. Dennard, and W. Haensch, “Practical strategies for power-efficient computing technologies,” *Proc. IEEE*, vol. 98, no. 2, pp. 215236, Feb. 2010.

[2] T. N. Theis, P. M. Solomon, “In quest of the “Next Switch”: Prospects for greatly reduced power dissipation in a successor to the silicon field-effect transistor,” *Proc. IEEE*, vol. 98, no. 12, pp. 20052014, Dec. 2010.

[3] S. Salahuddin, S. Datta, “Use of Negative Capacitance to Provide Voltage Amplification for Low Power Nanoscale Devices,” *Nano Lett.* vol. 8, no. 2, pp. 405-410, Dec. 2008.

[4] Y. Taur, T. H. Ning, *Fundamentals of Modern VLSI Devices*, 2nd *ed.*; Cambridge, UK: Cambridge University Press, 2009; Chap. 2, 3.

[5] J. D. Meindl, Q. Chen, J. A. Davis, “Limits on silicon nanoelectronics for terascale integration,” *Science*, vol. 293, no. 5537, pp. 20442049, Sep. 2001.

[6] W.Haensch, E. J.Nowak, R. H.Dennard, P. M. Solomon, A. Bryant,O. H. Dokumaci, A. Kumar, X. Wang, J. B. Johnson, and M. V. Fischett, “Silicon CMOS devices beyond scaling,” *IBM J. Res. Develop.*, vol. 50, no. 4/5, pp. 339361, Jul. 2006.

[7] R. K. Jana, G. Snider, and D. Jena, “Energy-Efficient Clocking Based on Resonant Switching for Low-Power Computation,” *IEEE Trans. Circuits Syst. I*, vol.61, no.5, pp.1400,1408, May 2014.

[8] R. Wang, G. Li, J. Verma, B. Sensale-Rodriguez, T. Fang, J. Guo, Z. Hu, O. Laboutin, Y. Cao, W. Johnson, G. Snider, P. Fay, D. Jena, and H. Xing, “220-GHz Quaternary Barrier InAlGaN/AlN/GaN HEMTs,” *IEEE Electron Dev. Lett.*, vol. 32, no. 9, pp. 1215, Sep. 2011.

[9] Z. Hu, R. Jana, M. Qi, S. Ganguly, B. Song, E. Kohn, D. Jena, and H. Xing, “Characteristics of $In_{0.17}Al_{0.83}N$/AlN/GaN MOSHEMTs with steeper than 60 mV/decade sub-threshold slopes in the deep sub-threshold region,” *Device Research Conference (DRC), 72*nd *Annual. IEEE.*, pp. 27-28, June 2014, doi: 10.1109/DRC.2014.6872283.

[10] T. van Hemert, D. Sarakiotis, S. Jose, R.J.E. Hueting, and J. Schmitz, “Exploring Capacitance-Voltage Measurements to find the Piezoelectric Coefficient of Aluminum Nitride,” *2011 IEEE Conference on Microelectronic Test Structures*, pp. 60-73, 2011.

[11] H. W. Then, et al., “Experimental Observation and Physics of ”Negative” Capacitance and Steeper than 40 mV/decade Subthreshold Swing in $Al_{0.83}In_{0.17}N$/AlN/GaN MOS-HEMT on SiC Substrate,” *Int. Electron Devices Meet. Tech. Dig.*, pp. 691694, 2013.

[12] R. K. Jana, G. Snider, and D. Jena, “On the possibility of sub-60 mV/decade subthreshold switching in piezoelectric gate barrier transistors,” *Phys. Status Solidi (c)*, vol. 10, pp. 1469-1472, Oct. 2013.

[13] R. K. Jana, G. Snider, and D. Jena, “Sub-Boltzmann transistors with piezoelectric gate barriers,” *Energy Efficient Electronic Systems (E3S), 3*rd *Berkeley Symposium on*, pp. 1-2, Oct. 2013, doi: 10.1109/E3S.2013.6705877.

[14] R. K. Jana, A. Ajoy, G. Snider, and D. Jena, “Sub-60 mV/decade Steep Transistors with Compliant Piezoelectric Gate Barriers,” *Int. Electron Devices Meet (IEDM). Tech. Dig.*, pp. 13.6.1 - 13.6.4, Dec. 2014, doi: 10.1109/IEDM.2014.7047047.

[15] R. E. Pelrine, R. D. Kornbluh, J. P. Joseph, “Electrostriction of polymer dielectrics with compliant electrodes as a means of actuation,” *Sens. and Actuators A Phys.*, vol. 64, pp. 77-84, Jan. 1998.

[16] C. Rivera, “Effects of electrostatic force on piezoelectric materials under high electric field: Impact on GaN-based nanoscale structures,” *J. Appl. Phys.*, vol. 109, pp. 013513, Jan. 2011.

[17] M. Akiyama, K. Umeda, A. Honda, and T. Nagase, “Influence of scandium concentration on power generation figure of merit of scandium aluminum nitride thin films,” *Appl. Phys. Lett.*, vol. 102, pp. 021915, 2013.

[18] F. Tasnadi, B. Alling, C. Hoglund, G. Wingqvist, J. Birch, L. Hultman, and I. A. Abrikosov, “Origin of the Anomalous Piezoelectric Response inWurtzite $Sc_xAl_{1-x}N$ Alloys,” *Phys. Rev. Lett.*, vol. 104, pp. 137601, 2010.

[19] M. Masuduzzaman and M. A. Alam. “Effective Nanometer Airgap of NEMS Devices Using Negative Capacitance of Ferroelectric Materials,” *Nano Lett.*, vol.14, pp. 3160-3165, 2014.

[20] A. Verma, S. Raghavan, S. Stemmer, and D. Jena, “Au-gated SrTiO3 field-effect transistors with large electron concentration and current modulation,” *Appl. Phys. Lett.*, vol. 105, pp. 113512, 2014.

[21] K. Natori, “Ballistic metal-oxide-semiconductor field effect transistor,” *J. Appl. Phys.*, vol. 76, pp. 4880, 1994.

[22] D. Jena, K. Banerjee, H. Xing, “2D crystal semiconductors: Intimate contacts,” *Nature Mater.*, vol. 13, pp. 1076, Nov. 2014.

[23] C. Wood, D. Jena, *Polarization Effects in Semiconductors: From Ab Initio Theory to Device Applications*; Springer: New York, 2008.

[24] H.-P. Chen, et al., “Modeling and Design of Ferroelectric MOSFETs,” *IEEE Trans. Electron Devices*, vol. 58, pp. 2401-2405, Aug. 2011.

[25] C. Cherry, “Some general theorems for nonlinear systems possessing reactance,” *Philos. Mag.*, vol. 42, no. 333, pp. 1161-1177, Oct. 1951.

[26] D. J. Frank, P. M. Solomon, C. Dubourdieu, M. M. Frank, V. Narayanan, and T. N. Theis, “The Quantum Metal Ferroelectric Field-Effect Transistor,” *IEEE Trans. Electron Devices*, vol. 61, no. 6, pp. 2145-2153, Jun. 2014.

Supporting Information
Transistor Switches using Active Piezoelectric Gate Barriers

S1. $\sigma_m - V$ RELATION OF PIEZOELECTRIC CAPACITOR WITH σ_{sp}

Following the same notation as the main text, the 4th order charge versus voltage $\sigma_m - V$ relation of an electromechanical capacitor is

$$C_0 V = \sigma_m - \sigma_{sp} + \frac{(\sigma_{sp} - e_{33})}{\epsilon_d C_{33}}\sigma_m^2 - \frac{1}{\epsilon_d C_{33}}\sigma_m^3 + \frac{e_{33}}{(\epsilon_d C_{33})^2}\sigma_m^4. \tag{S1}$$

The right side is a fourth order polynomial in σ_m, and captures the electromechanical coupling physics. Writing $\sigma_m = qn_m$ where n_m is the sheet charge density on the metal and $\sigma_{sp} = qn_{sp} \neq 0$, the polynomial factorizes to

$$C_0 V = qn_{sp}(1 - \frac{n_m}{n_\alpha^+})(\frac{n_m}{n_\alpha^-} - 1)(1 - \frac{n_m}{n_\eta})(1 + \frac{n_m}{n_\eta}), \tag{S2}$$

where $n_\alpha^+ = (n_\pi + \sqrt{n_\pi^2 - 4n_{sp}n_\pi})/2$, $n_\alpha^- = (n_\pi - \sqrt{n_\pi^2 - 4n_{sp}n_\pi})/2$, $qn_\pi = \epsilon_d C_{33}/e_{33}$, and $qn_\eta = \sqrt{\epsilon_d C_{33}}$. The four roots are characteristic sheet densities determined uniquely by the electromechanical coefficients and the spontaneous polarization of the dielectric material. If $n_\pi > 4n_{sp}$ which is met if $C_{33} > 4n_{sp}e_{33}/\epsilon_d$, then all four roots are real. The effect of spontaneous polarization $\sigma_{sp} \neq 0$ C/m^2 is a voltage offset, which leads to left and right shifts of the $qn_m - V$ characteristics (black and red curves) with respect to the characteristic (blue curve) with $\sigma_{sp} = 0$ C/m^2, as shown in Fig. S1. These shifts will move the threshold voltages of a corresponding transistor, and will also locally change the slopes of the charge-voltage characteristics.

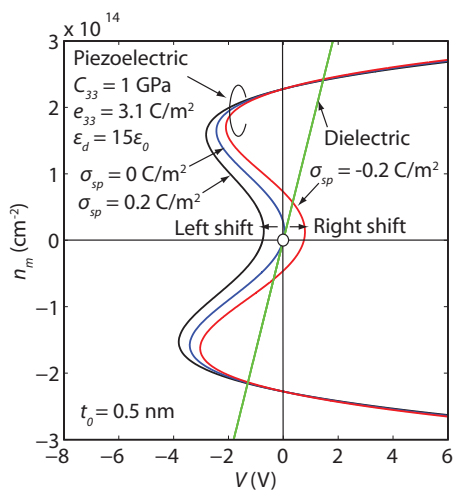

Fig. S1. Charge-voltage ($qn_m - V$) characteristics of an electromechanical capacitor with piezoelectric barrier. Color lines (black, blue and red) show the characteristics of capacitors for $\sigma_{sp} = 0.2$ C/m^2, 0 C/m^2, and -0.2 C/m^2. $\sigma_{sp} \neq 0$ C/m^2 leads to horizontal left and right shifts of $qn_m - V$ curve.

S2. BALLISTIC FET I-V MODEL

When no drain voltage is applied, carriers in the semiconductor are in thermal equilibrium with the source and drain reservoirs, which for a parabolic 2D bandstructure means $qn_s = C_{sc}V_{th}\ln(1 + \exp[(E_{Fs} - E_c)/kT])$. From the energy band diagram of metal-piezoelectric-semiconductor stack of a transistor (Fig. S2), the voltage division $qV_{gs}^{'} = qV + (E_{Fs}^0 - E_c)$ translates to the dimensionless equation,

$$e^{\frac{V_{gs}}{V_{th}}} = e^{\frac{qF(n_s)}{C_0 V_{th}}}(e^{\frac{qn_s}{C_q V_{th}}} - 1), \tag{S3}$$

where we have defined $F(n_s) = n_{sp}(1 - \frac{n_s}{n_\alpha^+})(\frac{n_s}{n_\alpha^-} - 1)(1 - \frac{n_s}{n_\eta})(1 + \frac{n_s}{n_\eta})$. This equation must be solved to find the semiconductor charge n_s at a gate voltage V_{gs}. If the dielectric is piezoelectric but does not have spontaneous polarization, one must replace $F(n_s)$ by $F_{pz}(n_s) = n_s(1 - \frac{n_s}{n_\eta})(1 + \frac{n_s}{n_\eta})(1 - \frac{n_s}{n_\pi})$ to find the semiconductor charge in response to the gate voltage. This is the major change to a standard Natori-type ballistic FET model [1] brought about by the piezoelectric gate barrier.

When a drain voltage V_{ds} is applied, the carrier distribution in the 'top-of-the-barrier' point x_{max} in the energy band diagram is split in two. In the ballistic limit of transport, the right-going carriers are in equilibrium with the source reservoir of Fermi energy E_{Fs}, whereas the left-going carriers are in equilibrium with the drain reservoir E_{Fd}, and they are out of equilibrium by $E_{Fs} - E_{Fd} = qV_{ds}^{'}$. Note that $E_{Fs}^0 \neq E_{Fs}$; the application of a drain bias causes a rearrangement of the carrier distribution

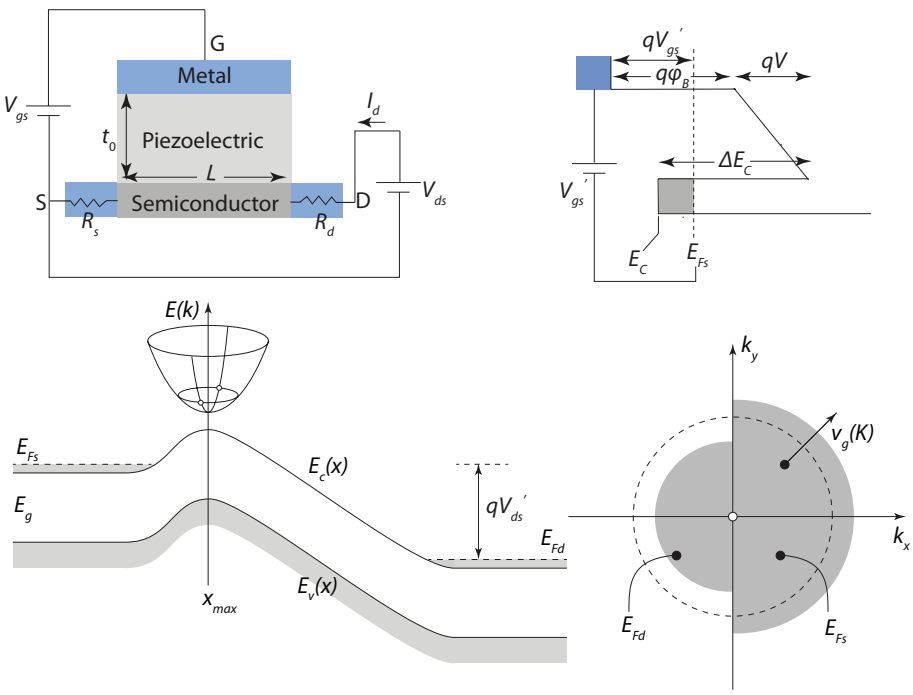

Fig. S2. Schematic cross section of a transistor ("piezoFET") with a piezoelectric gate barrier, semiconductor channel such as Si, GaN or 2D material, MoS_2 and source and drain ohmic contacts. Energy band diagram for the metal-piezoelectric-semiconductor stack of the transistor. For transistor operation, we use ballistic transport model to calculate the transistor characteristics. The mobile sheet carrier density at the 'top-of-the-barrier' in energy band diagram is controlled by V_{gs} through the piezoelectric gate barrier, and source and drain Fermi levels E_{Fs} & E_{Fd} are separated by V_{ds}. Dashed circle shows the k-space for carrier distributions at $V_{ds} = 0$ and grey circle shows the k-space for carrier distributions at applied $V_{ds}^{'}$ i.e. $E_{Fs} - E_{Fd} = qV_{ds}^{'}$. $v_g(k)$ is the group velocity of carriers. Here, $V_{ds}^{'} = V_{ds} - I_d(R_s + R_d)$, where R_s and R_d are the source and drain contact resistances.

in the semiconductor channel. However, with good electrostatic design, one can ensure that the *net* carrier density at x_{max} is the same as when $V_{ds}^{'} = 0$. The carrier distribution in the $k-$space is depicted in Fig. S2; the dashed circle is the distribution for $V_{ds}^{'} = 0$, and the gray half-circles are the result of application of a drain bias, both in the $T \to 0$ K limit. Defining $\eta_s = (E_{Fs} - E_c)/kT$, $v_d = V_{ds}^{'}/kT$, we find that for maintaining the same carrier density, one must meet the condition $qn_s = \frac{1}{2}C_q V_{th} \ln(1 + e^{\eta_s})(1 + e^{\eta_s - v_d})$, which yields

$$\eta_s = \ln[\sqrt{(1 + e^{v_d})^2 + 4e^{v_d}(e^{\frac{2qn_s}{C_q V_{th}}} - 1)} - (1 + e^{v_d})] - \ln[2] \tag{S4}$$

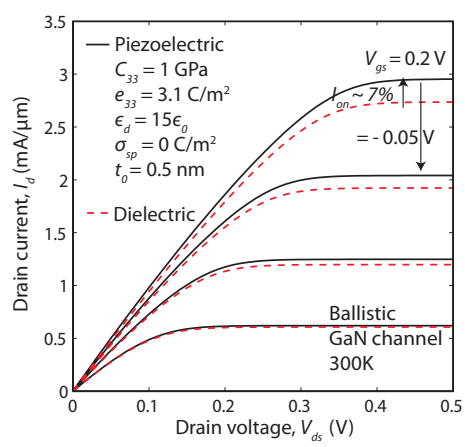

Fig. S3. Output characteristics depicts the drain current I_d versus V_{ds} at gate bias voltage $V_{gs} = 0.2$ V with a step of -0.05 V for GaN piezoFETs with piezoelectric (solid line) and dielectric barriers (dashed line). A boost in the on-current is obtained for transistor with a compliant piezoelectric barrier than a dielectric one.

Note that this is of a similar form as the seminal result on ballistic transistors by Natori et al [1], but the factor n_s inside the square root must be obtained from Eq. S3 to account for the electromechanical coupling self-consistently. By summing

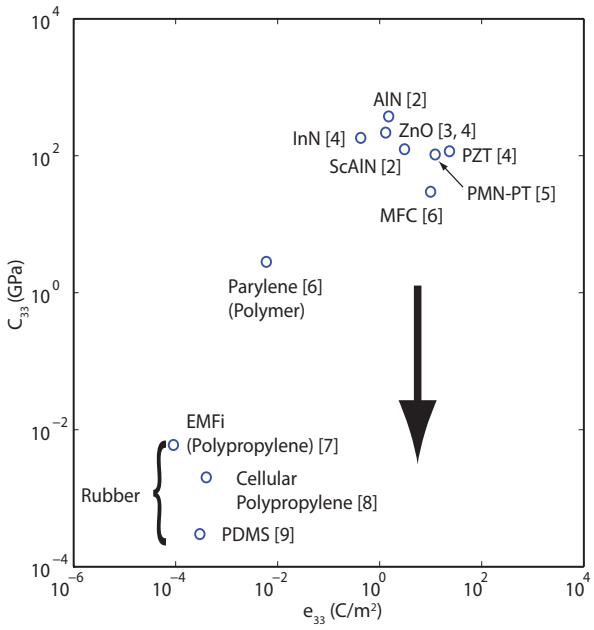

Piezoelectric	C_{33} (GPa)	e_{33} (C/m²)	References
AlN	375	1.5	[2]
ScAlN	125	3.1	[2]
ZnO	218	1.32	[3, 4]
InN	182	0.43	[4]
PZT5H	117	23.3	[4]
PMN-PT	105	12.2	[5]
MFC (Macro-fiber composite)	30	10.6	[6]
Parylene (polymer)	2.8	0.006	[6]
EMFi (Polypropylene)	0.006	0.00009	[7]
Cellular Polypropylene	0.002	0.0004	[8]
PDMS	0.0003	0.0003	[9]

Fig. S4. Piezoelectric Materials with C_{33} and e_{33} coefficients. Table for different C_{33} and e_{33} coefficients of various piezoelectrics with corresponding references. C_{33} and e_{33} values are obtained by literature review from listed references. e_{33} is extracted from a matrix relation of $[e] = [C] * [d]$ where $[e]$ (unit: C/m^2) is the piezoelectric coefficient matrix, $[C]$ (unit: N/m^2) is the elastic stiffness matrix, [d] (unit: C/N) is the piezoelectric coupling matrix. These matrices have sparsity pattern depends on the symmetry of the crystal. However, here in order to get an estimation of the magnitude of e_{33}, we use a simpler relation e_{33} (C/m^2) $= C_{33}$ (N/m^2) $* \, d_{33}$ (C/N), in cases where e_{33} is not quoted in references. The arrow shows the desired piezoelectric materials to be used for gate barriers of steep transistors.

over the group velocities of the $k-$states, the net current per unit width of the ballistic piezoFET is then given by the same expression as in Natori [1]:

$$J = J_0 \left(F_{\frac{1}{2}}(\eta_s) - F_{\frac{1}{2}}(\eta_s - \eta_d) \right) \tag{S5}$$

where $J_0 = \frac{q g_s g_v \sqrt{2m^\star}(kT)^{\frac{3}{2}}}{2\pi\hbar^2}$, and $F_{\frac{1}{2}}$ is the Fermi-Dirac integral of order $1/2$.

The above expressions provide the complete electrical characteristics of a ballistic piezoFET at any temperature in a compact model. We can obtain n_s at any gate voltage V_{gs} fully accounting for the electromechanical coupling by solving Eq. S3. We then find η_s at any given V_{gs} and V_{ds} using Eq. S4, and finally find the drain current per unit width using Eq. S5. Fig. S3 shows the output characteristics depicting $I_d - V_{ds}$ at different V_{gs} for GaN channel transistors with a compliant piezoelectric (solid lines) and passive dielectric (dashed lines) barriers.

Fig. S4 describes different piezoelectric materials with C_{33} and e_{33} coefficients obtained by literature review from Refs. [2], [3], [4], [5], [6], [7], [8], [9]. Compliant piezoelectric materials with parameter space such as lower C_{33} (higher compliance), and higher e_{33} (higher piezoelectricity), shown by the arrow in Fig. S4 are useful for gate barriers of proposed steep transistors.

S3. Energy landscape for piezoelectric-semiconductor stack: Computational Details

A. Definition of Free-Energy

Consider the circuit in Fig. S5, showing a piezoelectric-semiconductor stack connected to a voltage source via a resistor R (units: Ωcm^2). Both the piezoelectric insulator and semiconductor have non-linear charge (σ_m) - voltage (V) characteristics, denoted say by $V = V_{ins} = f_1(\sigma_m)$ and $\psi_s = f_2(\sigma_m)$ respectively. A systematic method of studying the behavior of circuits with non-linear elements uses the Euler-Lagrange equations [10]:

$$\mathcal{L}(\sigma_m, \dot{\sigma}_m) = T' - U \tag{S6}$$

$$U(\sigma_m) = \int_0^{\sigma_m} f_1(\tilde{\sigma}_m) d\tilde{\sigma}_m + \int_0^{\sigma_m} f_2(\tilde{\sigma}_m) d\tilde{\sigma}_m \tag{S7}$$

$$\frac{d\sigma_m}{dt}\left(\frac{\partial \mathcal{L}}{\partial \dot{\sigma}_m}\right) - \frac{\partial \mathcal{L}}{\partial \sigma_m} = V_{gs}^{'} - R\dot{\sigma}_m, \tag{S8}$$

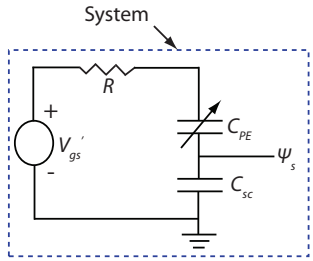

Fig. S5. Schematic of a system shows a piezoelectric-semiconductor stack, represented by a series combination of piezoelectric capacitance C_{PE} and semiconductor capacitance C_{sc} connected to $V_{gs}^{'}$ via a resistor R. ψ_s is the channel surface potential at the insulator-semiconductor interface.

where $\mathcal{L}(\sigma_m, \dot{\sigma}_m)$ is the Lagrangian, $T'(\dot{\sigma}_m)$ is the magnetic co-energy (in any inductors) and $U(\dot{\sigma}_m)$ is the potential energy in the capacitors in the circuit. For the circuit in Fig. S5, $T' = 0$, and we have

$$f_1(\sigma_m) + f_2(\sigma_m) = V_{gs}^{'} - R\dot{\sigma}_m, \tag{S9}$$

which under equilibrium ($\dot{\sigma}_m = 0$) gives $V_{gs}' = f_1(\sigma_{m_0}) + f_2(\sigma_{m_0})$. To determine whether σ_{m_0} is a point of stable/unstable equilibrium, we write $\sigma_m = \sigma_{m_0} + \delta\sigma_{m_0}$ for a small perturbation $\delta\sigma_{m_0}$, expand the Lagrangian as a Taylor series (upto second order) about σ_{m_0}, and analyze whether the perturbation grows or decays with time:

$$\delta\dot{\sigma}_m = -2\frac{f_1'(\sigma_{m_0}) + f_2'(\sigma_{m_0})}{R}\delta\sigma_m = -\delta\sigma_m/\tau \tag{S10}$$

$$\delta\sigma_m(t) = \delta\sigma_{m_0}\exp(-t/\tau). \tag{S11}$$

where $f'(\sigma_m)$ is the derivative of $f(\sigma_m)$ w.r.t σ_m. The system is stable to perturbations if $\delta\sigma_m(t) \to 0$ as $t \to 0$, i.e. if $f_1'(\sigma_{m_0}) + f_2'(\sigma_{m_0}) > 0$. The above discussion motivates the definition of the free-energy $G(\sigma_m)$:

$$G(\sigma_m, V_{gs}^{'}) = \int_0^{\sigma_m} \left[f_1(\tilde{\sigma}_m) + f_2(\tilde{\sigma}_m)\right] d\tilde{\sigma}_m - \sigma_m V_{gs}^{'}. \tag{S12}$$

From the carrier density expression in a semiconductor channel, ψ_s can be expressed as $\psi_s = f_2(\tilde{\sigma_m}) = V_{th}\ln\left(e^{\frac{\tilde{\sigma_m}}{C_{sc}V_{th}}} - 1\right)$. Using the expressions of ψ_s and $V_{ins} = f_1(\tilde{\sigma_m})$ in Eq. S12, the free energy G (unit: J/m^2) is found to be

$$\begin{aligned} G = \alpha_5\sigma_m^5 + \alpha_4\sigma_m^4 + \alpha_3\sigma_m^3 + \alpha_2\sigma_m^2 \\ + V_{th}\int_0^{\sigma_m} \ln\left(e^{\frac{\tilde{\sigma}_m}{C_{sc}V_{th}}} - 1\right) d\tilde{\sigma}_m - \sigma_m V_{gs}^{'}, \end{aligned} \tag{S13}$$

where $\alpha_5 = \frac{e_{33}}{5C_0(\epsilon_d C_{33})^2}$, $\alpha_4 = \frac{1}{4C_0\epsilon_d C_{33}}$, $\alpha_3 = \frac{(\sigma_{sp} - e_{33})}{3C_0\epsilon_d C_{33}}$, $\alpha_2 = \frac{1}{2C_0}$ are material and geometric constants of the problem. Note the internal energy is a non-linear function of the sheet charge σ_m, and is a linear function of applied gate bias voltage V_{gs}. Then, all points of equilibrium satisfy $\partial G/\partial\sigma_m = 0$, and further, points of *stable* equilibrium satisfy $\partial^2 G/\partial\sigma_m^2 > 0$.

B. Self-consistent solution

We make use of the Euler-Lagrange equation to calculate the $I - V$ characteristics of the PiezoFET. The basic structure of the self-consistent algorithm involves an outer loop that determines the voltage drop across the intrinsic FET (i.e eliminating the voltage drops across the contacts). Inside this loop, we require the charge n_s for the intrinsic gate voltage. To do this, we solve the Euler-Lagrange equation (using the implicit Euler method for about 5τ) to determine a good guess of charge $n_{s,guess}$ at the present voltage, starting from the value of n_{s0} obtained at a previous voltage. $n_{s,guess}$ is then used in a fixed point iteration scheme to determine n_s, from which the current is finally calculated. We have not encountered prior use of this Euler-Lagrange method for the calculation of hysteretic characteristics of electron device systems in an extensive literature search, and intend to publish the detailed procedure in a follow-up report.

REFERENCES

[1] K. Natori, "Ballistic metal-oxide-semiconductor field effect transistor," *J. Appl. Phys.*, vol. 76, pp. 4880, 1994.

[2] F. Tasnadi, B. Alling, C. Hoglund, G. Wingqvist, J. Birch, L. Hultman, and I. A. Abrikosov, "Origin of the Anomalous Piezoelectric Response inWurtzite $Sc_xAl_{1-x}N$ Alloys," *Phys. Rev. Lett.*, vol. 104, pp. 137601, 2010.

[3] K. Umeda, H. Kawai, A. Honda, M. Akiyama, T. Kato, T. Fukura, "Piezoelectric properties of ScAlN thin films for piezo-MEMS devices," *Micro Electro Mechanical Systems (MEMS), 2013 IEEE 26th International Conference on.*, pp. 733-736, Jan 2013.

[4] S. Wilson, "*New materials for micro-scale sensors and actuators. An engineering review*", *Materials Science and Engineering. R, Reports*, vol. 56, no. 1-6, pp. 1-229, June 2007, table 3.1 (page-27).

[5] H. Cao, V. H. Schmidt, R. Zhang, W. Cao, and H. Luo, “Elastic, piezoelectric, and dielectric properties of 0.58Pb($Mg_{1/3}Nb_{2/3}$)O_3 - 0.42$PbTiO_3$ single crystal,” *J. Appl. Phys.*, vol. 96, no. 1, pp. 549-554, July 2004.

[6] K. S. Ramadan, D. Sameoto, and S. Evoy, “A review of piezoelectric polymers as functional materials for electromechanical transducers,” *Smart Mater. Struct.*, vol. 23, pp. 033001, Jan. 2014.

[7] R. Kressmanna, “New piezoelectric polymer for air-borne and water-borne sound transducers,” *J. Acoust. Soc. Am.*, vol. 109, no. 4, pp. 1412, April 2001.

[8] W. Heywang, K. Lubitz, W. Wersing, “*Piezoelectricity: Evolution and Future of a Technology*”; Springer: Verlag Berlin Heidelberg, 2008, chapter-6, table 6.1.

[9] J.-J. Wang, J.-W. Tsai, and Y.-C. Su, “Piezoelectric rubber films for highly sensitive impact measurement,” *J. Micromech. Microeng.*, vol. 23, pp. 075009, May 2013.

[10] C. Cherry, “Some general theorems for nonlinear systems possessing reactance,” *Philos. Mag.*, vol. 42, no. 333, pp. 1161-1177, Oct. 1951.